AN OVERVIEW OF THE EVALUATION OF OXYGEN INTERACTION WITH MATERIALS—THIRD PHASE (EOIM-III) EXPERIMENT: SPACE SHUTTLE MISSION 46

Lubert J. Leger, Steven L. Koontz, James T. Visentine and Donald Hunton

ABSTRACT

The interaction of the atomic oxygen (AO) component of the low-Earth orbit (LEO) environment with spacecraft materials has been the subject of several flight experiments over the past 11 years. The effect of AO interactions with materials has been shown to be significant for long-lived spacecraft such as Space Station *Freedom* (S.S. *Freedom*) and has resulted in materials changes for externally exposed surfaces. The data obtained from previous flight experiments, augmented by limited ground-based evaluations, have been used to evaluate hardware performance and select materials. Questions pertaining to the accuracy of this data base remain, resulting from the use of long-term ambient density models to estimate the O-atom fluxes and fluences needed to calculate materials reactivity in short-term flight experiments. The EOIM-III flight experiment was designed to produce benchmark AO reactivity data and was carried out during STS-46. Ambient density measurements were made with a quadrupole mass spectrometer which was calibrated for AO measurements in a unique ground-based test facility. The combination of these data with the predictions of ambient density models allows an assessment of the accuracy of measured reaction rates on a wide variety of materials, many of which had never been tested in LEO before. The mass spectrometer is also used to obtain a better definition of the local neutral and plasma environments resulting from interaction of the ambient atmosphere with various spacecraft surfaces. In addition, the EOIM-III experiment was designed to produce information on the effects of temperature, mechanical stress, and solar exposure on the AO reactivity of a wide range of materials. An overview of EOIM-III methods and results are presented in this paper.

INTRODUCTION

The external surfaces of spacecraft in the LEO (200 to 500 km) environment are exposed to a number of natural environmental factors capable of degrading spacecraft materials and spacecraft performance. AO, solar ultraviolet (UV) and vacuum ultraviolet (VUV) radiation, ionizing radiation, plasma interactions, thermal cycling, and micrometeoroids/debris can all contribute to spacecraft performance degradation to varying degrees depending on spacecraft orientation, orbital inclination, orbital altitude, and state of the solar cycle (refs. 1–3). AO is the major constituent of the natural atmospheric environment in LEO and has been shown to be one of the most important factors in the environmental degradation of several important classes of spacecraft materials in a series of flight experiments and laboratory studies conducted over the past 11 years (refs. 4–8). The data from these experiments have, along with 10- to 30-year life requirements, driven a number of materials selections for S.S. *Freedom* such as: (1) SiO_x protective coatings for Kapton™ solar array blankets, (2) O-atom/UV resistant multilayer insulation blankets, and (3) anodized aluminum coatings.

In addition, the interaction of the natural environment with spacecraft surfaces creates local induced environments which can have an impact on vehicle performance and mission success.

Examples include spacecraft glow and the ram-density or bow wave effect. Spacecraft in LEO travel through the ambient environment at high velocity so that forward-facing surfaces receive a constant flux of high-velocity atoms and molecules which lose kinetic energy on inelastic collision with those surfaces. The result is a buildup of thermalized ambient species and surface reaction products ahead of the spacecraft and especially around any ram-oriented spacecraft surfaces (ram surfaces are oriented perpendicular to the velocity vector, facing forward). Spacecraft glow (refs. 9,10) and ram density (ref. 11) are examples of local induced environment effects which can influence Earth observation and astrophysical measurements.

An understanding of the surface chemistry which gives rise to materials degradation and induced environment effects in LEO is essential for the design of reliable long-lived LEO spacecraft such as S.S. *Freedom*. The LEO AO reactivities of materials measured before EOIM-III are based on AO fluences calculated using the MSIS-86 model of the thermosphere (ref. 12). Predictions made using MSIS-86 can have errors of up to ±25 percent because the inputs used in the calculations are averages taken over various time periods rather than instantaneous values (ref. 13). As a result, the uncertainty in the O-atom fluence propagates directly to become uncertainty in measured reactivities. Similar limitations apply to modeling and prediction of induced environments.

The primary objective of the EOIM-III flight experiment is to produce benchmark AO reactivity and induced environment data. The AO flux and fluence measured during the period of materials exposure is compared with MSIS-86-based calculations (ref. 13). The secondary objectives of EOIM-III include: (1) characterization of the induced microenvironment near several surfaces; (2) acquisition of basic chemistry data related to reaction mechanism; (3) determining the effects of surface temperature, mechanical stress, atom fluence, and solar UV/VUV radiation exposure on materials reactivity; and (4) characterization of the induced environment in the space shuttle cargo bay in a variety of flight orientations.

Our approach to achieving the EOIM-III objectives employed developing a ground-based mass spectrometer calibration facility which reproduces both the chemistry and rarefied gas dynamics of the LEO environment so that the mass spectrometer could be calibrated accurately before flight. As a result, quantitative measurements of both natural and induced environments could be made with confidence, satisfying the primary objective and many of the secondary objectives. The remaining secondary objectives were achieved using a physical organic chemistry approach, i.e., a number of polymeric materials were exposed to the same O-atom environment in LEO to determine O-atom reactivity as a function of temperature, solar UV/VUV radiation dose, mechanical stress, polymer molecular structure, and formulation. While the Johnson Space Center (JSC) portion of EOIM-III emphasized polymers and S.S. *Freedom* materials candidates, other investigator teams selected inorganic, metallic, or composite materials. However, the same reasoning, i.e. reactivity as a function of material structure, composition, and temperature for a single well-defined O-atom dose, still applies.

The EIOM-III experiment was carried out during STS-46 (late August 1992) in the Space Shuttle *Atlantis* at an orbital altitude of 123 to 124 nmi to maximize the O-atom fluence obtained in a 42-h exposure. The inclination of the orbit was 28.5°. The shuttle was oriented so that the cargo bay normal was within ±2° of the velocity vector so that the experiment was in AO ram for 42 h. A standard air-to-ground telemetry link combined with a telemetry work station permitted the display and analysis of data during the mission.

EOIM-III was a team effort involving not only NASA Centers but also the U.S. Air Force Phillips Laboratories, the Aerospace Corporation, the University of Alabama in Huntsville, and the S.S. *Freedom* contractor team. International participation included the National Space Agency of

Japan, the European Space Agency (ESA), and the Canadian Space Agency. This paper reports only the preliminary results from the JSC and Air Force Phillips Laboratory portion of the experiment.

EOIM-III FLIGHT EXPERIMENT HARDWARE

Photographs of the EOIM-III experiment hardware after installation in the Space Shuttle *Atlantis* are shown in Figures 1 and 2. The cargo bay aft bulkhead is visible at the top of Figures 1 and 2. EOIM-III is on the left and Thermal Energy Management Processes 2A3 (TEMP-2A3) on the right of the supporting white framework (IMPESS structure) as viewed in the photographs. The payload at the bottom of Figure 1 is the ESA Retrievable Carrier (EURECA) satellite. EOIM-III is in flight configuration with all protective covers removed. Figure 3 is a line drawing of the EOIM-III payload which identifies the various subexperiments and assemblies and should be used as a key to identify the various features in Figures 1 and 2. Figure 4 is a line drawing showing the cargo bay configuration of *Atlantis* for STS-46.

The passive sample carriers, rectangular trays with circular openings, are visible on the left hand, forward side of Figure 2, with composite stress fixtures, a polymer film stress fixture, and a scatterometer assembly toward the back. In the center portion of the experiment, moving from fore to aft (away from the viewer), we have a S.S. *Freedom* Solar Array Materials Experiment (SSFAME, the brown rectangle), the mass spectrometer carousel, and finally the mass spectrometer itself, the metallic cylinder pointing along the cargo bay normal (-Z axis in space shuttle orbiter coordinates). The right-hand side of the experiment holds three heated trays, rectangular trays with small openings, which were thermostated at 200 °C (fore), 120 °C (center), and 60 °C (aft) during the 42-h AO ram exposure period. Also on the right-hand side are additional polymer film stress fixtures, scatterometers, the AO Monitor (AOM), the temperature-controlled quartz crystal microbalances (TQCM's) in the Environmental Monitoring Package (EMP), the Variable Exposure Tray (VET) assembly and the Solar UV Tray (SUV) assembly. The temperatures of specific locations on the passive and heated tray sets as well as the payload pallet and the mass spectrometer were measured throughout the mission.

Samples in the passive carriers, the heated trays, and the SUV and VET were characterized before and after the EOIM-III exposure; and oxygen reactivity was calculated from sample property change and total atom fluence. The relationship between property change and atom fluence is not linear in all cases. Specific characterization techniques and data interpretation vary with the materials and the choices of the investigator teams. The polymeric materials selected by the JSC team were characterized by: (1) mass loss measured by weighing the AO samples and controls before and after flight, (2) surface recession as determined by profilometry and/or scanning electron microscopy, and (3) bulk and surface chemistry changes as determined by Fourier transform infrared spectroscopy and x-ray photoelectron spectroscopy. All AO samples and controls were baked in a vacuum of 10^{-7} torr or better for at least 48 h at the expected on-orbit temperature. Sample surfaces were then cleaned by rinsing with Optisolv (QClean Systems, Monrovia, CA), a low-nonvolatile residue solvent, and air drying in a desiccator prior to installation in the sample trays. Samples were tested for compatibility with Optisolv. A high-transparency, stainless-steel, electroetched grid (Interconics, St. Paul, MN) was placed over each polymer sample to serve as an etch mask. The resulting periodic O-atom etch pattern made accurate profilometry possible despite the presence of natural surface irregularities. The preflight vacuum bakeout procedure was repeated before the postflight weighings, albeit without the solvent rinse.

The VET and SUV trays were equipped with movable covers. The VET tray was designed to progressively uncover a series of sample trays during the 42-h exposure period so that each tray experienced a different O-atom fluence. As described in the results section, the VET cover failed to operate properly during the mission and all sample trays received nearly identical exposures. The cover on the SUV tray covered one sample tray whenever solar UV/VUV radiation was present, so that one tray received O-atoms with UV/VUV, the other received O-atoms only, and a control tray was subjected to the same exposure as the passive trays.

The AOM and EMP subexperiments were designed to monitor both AO flux and molecular contamination by reporting near real time O-atom reaction rates with various materials or rate of mass deposition. The EMP consisted of five TQCM sensors, one of which had no reactive coating while the remaining three were coated with amorphous carbon, TFE Teflon™, a polyurethane, and a polyimide respectively. The AOM consisted of several vapor deposited carbon resistors. AO reaction with the carbon resistors produces a decrease in conductance as carbon is removed.

The mass spectrometer/carousel assembly was the key component of the EOIM-III flight experiment. The Air Force quadrupole mass spectrometer (ref. 14) was capable of sampling either the local neutral environment while rejecting naturally occurring ionic species (MODE-2) or measuring ionic species while rejecting the neutrals (MODE-1). The mass scan range was 2 to 80 amu and was scanned every 5 s. The mass spectrometer was equipped with a copper/beryllium dynode secondary electron multiplier having a gain of about 10^6 for detection of mass analyzed ions. The output current of the secondary electron amplifier was fed into a logarithmic amplifier which compressed 7 orders of magnitude of multiplier current into a 0 to 5 V output voltage which was digitized as an 8 bit binary integer, MS02 (0 to 256 = 0 to 5 V). The binary integer voltage (MS02) was converted to a linear multiplier current display using the formula,

$$I_{amps} = 10^{(-12.372+1.386*MS02*5/256)}.$$

The mission team could display mass spectra with either linear or logarithmic scales using the telemetry workstation.

The quardupole mass spectrometer was flown on a rotating mount so that the mass spectrometer sampling aperture could be pointed either directly out of the cargo bay (-Z direction as shown in Figures 1 to 4) or, after rotating 90° (+X direction), directly at one of the carousel sectors. When pointed in the -Z direction, the mass spectrometer is configured to make ambient density measurements whenever the cargo bay normal is ram oriented (-Z into the velocity vector). When pointed at a carousel sector, measurements of local induced environment were made. During the 42-h EOIM cycle the mass spectrometer and carousel assembly were operated according to a preprogrammed time sequence in which measurements of ambient neutrals, ambient ions, and the local induced environment in several carousel sectors were made in sequence during every 8-h EOIM cycle. Local induced environment effects measurements were made both with the carousel sector directly exposed to incoming ambient ram flux and with a movable baffle covering the sector being observed. The surfaces of each carousel sector were coated with a different material: (1) Z-306 black paint, (2) anodized aluminum, (3) ^{13}C Kapton™ polyimide, (4) Parylene-C, and (5) FEP Teflon™. Anodized aluminum and Teflon™ are common external surface types on S.S. *Freedom* as presently configured. Z-306 black paint is known to produce significant amounts of spacecraft glow when interacting with the ambient atmosphere (ram orientation) in LEO. Both ^{13}C Kapton™ Polyimide and Parylene-C are reactive organic polymers containing mass labels that permit easy mass spectrometric detection of gaseous reaction products in the presence of natural

orbiter and instrument background gases; ^{13}CO and $^{13}CO_2$ in the case of the labeled Kapton™ and Cl, COCl, and other chlorine containing in the case of Parylene-C.

Preflight calibration of the EOIM-III mass spectrometer was conducted at Los Alamos National Laboratories using techniques which have been previously reported (ref. 15). It should be noted that the calibration factors reported in reference 15 were not those used during the mission. The Air Force mass spectrometer was cleaned, refurbished, and recalibrated prior to EOIM-III, and small changes in the calibration factors were noted. Postflight calibration is in progress at Los Alamos, and a complete description of calibration and mass spectrometer performance will be published separately. Briefly, the flight mass spectrometer was calibrated for thermalized gases using a spinning rotor gauge (molecular drag gauge) which had been subjected to a National Institutes of Science and Technology traceable calibration. The same spinning rotor gauge was used to support quantitative calculation of the flux of oxygen atoms in the high-velocity neutral O-atom beam, permitting calibration for ram flux measurements on orbit. Preliminary postflight calibration of the Air Force mass spectrometer has shown no significant change in calibration factors thus far. It should be noted that mass peak areas, not peak heights, were used for all measurements. Also, mass 16 peak areas (AO) were corrected for contributions resulting from mass 16 fragments produced by higher mass species such as H_2O, O_2,and CO_2.

EOIM-III FLIGHT EXPERIMENT PROCEDURES AND ENVIRONMENTS

The EOIM-III payload was activated in stages. Primary electrical power was applied about 2 h after opening the cargo bay doors. Telemetry was then enabled so that temperature and EMP data were transmitted for the rest of the mission. The mass spectrometer was operated intermittently before EOIM-III was initiated to obtain natural and induced environment data for selected vehicle attitudes and altitudes. Ambient neutral and ionic density measurements were conducted at altitudes of 231, 160, and 124 nmi. The mass spectrometer was pointed in the -Z direction for all measurements made prior to EOIM-III with MODE-1 (ambient ions) and MODE-2 (ambient neutrals) measurements made during alternate 1-min time periods.

EOIM-III was performed toward the end of the STS-46 mission, after the orbital altitude was reduced to 123 to 124 nmi and the inclination ramained fixed at 28.5°. Data were collected and telemetered continuously for several preprogrammed measurement cycles. Just prior to powering down the EOIM-III payload, *Atlantis* was put through a roll around the orbiter X-axis, moving the mass spectrometer from ram to deep wake and back into ram again to obtain data on the induced environment at various angles of attack. Mass spectrometer data were collected continuously during the roll maneuver, with the mass spectrometer taking neutral mass spectra (MODE-2) while pointed in the -Z direction. The EOIM-III vehicle orientation and orbital path are illustrated in Figure 5. Orbital inclination was 28.5°, with a beta angle (the angle between the Earth-Sun vector and the plane of the orbit) between 17.5° and 24.3°.

EOIM-III environmental exposure is summarized in Table 1. AO fluences were calculated using the MSIS-86 model of the thermosphere combined with an orbital mechanics package (Runflux) developed at JSC (ref. 16). The O-atom fluence values reported in Table 1 are provisional in that a significant increase in solar activity was observed during the EOIM-III experiment so that the usual monthly average values of the solar activity parameters are probably inappropriate. In addition, there is evidence of geomagnetic storm activity during STS-46 which suggests that the version of MSIS-86, capable of accounting for the enhanced nitrogen and argon densities which occur

during such storms, should be used. Final O-atom fluence values will be reported at a later date, although the increase in fluence should be less than 10 percent of the values reported in Table 1. An important feature of Table 1 is the 11.27-h period of solar inertial exposure associated with Eureka deployment and checkout. Solar inertial (cargo bay to the sun) is a high temperature attitude which also results in a significant solar UV/VUV radiation dose. The EOIM-III samples which were not covered during this time period (all samples except VET and SUV tray specimens which were under movable covers at the time) received a UV/VUV radiation dose greater than that received during the rest of the mission. Figures 6 and 7 show O-atom density (calculated using the methods of reference 16) as a function of time during the post EURECA deployment and EOIM-III portions of STS-46, respectively.

RESULTS AND DISCUSSION

Flight instrumentation generally performed well during EOIM-III. The Air Force mass spectrometer generated approximately 48,000 neutral and ion spectra. Mass spectra were collected at three different altitudes (124, 160, and 231 nmi), and included both ram and wake orientations of the orbiter cargo bay, vehicle roll maneuvers, shuttle engine firings, and support of Tethered Satellite System-1 operations. The EMP measured large deposition rates which correlated with ambient ram incident of the TQCM sensor. Postflight analysis shows thick deposits of SiO_x on the sensor surfaces which are not consistent with the low levels of contamination measured in an x-ray photoelectron spectroscopy survey of the EOIM-III payload (Table 2). The AOM functioned properly, showing a linear decrease in electrical conductance with increasing O-atom fluence and no evidence of increasing contamination levels. The cover on the VET experiment did not function as programmed; all three covered trays received the same O-atom fluence. The SUV and heated trays both functioned correctly. Finally, two switching problems were encountered which have not been explained. First, the mass spectrometer did not power-off properly after first power-on early in the mission resulting in an unplanned 13.6-h operation period. Second, the preprogrammed mass spectrometer/carousel cycle failed to initiate properly so that the first series of carousel measurements were delayed by about 6 h.

Mass Spectrometer/Carousel

As of this writing, only a limited amount of the mass spectral data has been reduced. As shown in Table 1, agreement between the calculated atom fluence and the mass spectrometer data from a limited number of orbits is satisfactory, confirming, at least qualitatively, the accuracy of the methods of reference 16 for this application and, therefore, the existing space shuttle AO reactivity data base.

Typical mass spectrometric measurements (MODE-2, neutrals) of ram flux taken at 231, 160, and 124 nmi altitudes are shown in Figures 8, 9, and 10, respectively. Several features of these spectra are a result of the induced environment in the ram oriented shuttle cargo bay and the mass spectrometer itself. The close proximity of the cargo bay aft bulkhead and the mass spectrometer (Figures 1 to 4) means that thermalized cargo bay gases can easily reach the mass spectrometer sampling aperture or the carousel sectors simply by scattering off (or desorbing from) the aft bulkhead. Water is not a significant component of the natural environment at 231 nmi but is the base peak in Figure 8. The water is not related to a specific dump event and is most likely due to cargo

bay and/or mass spectrometer outgassing. The molecular nitrogen and oxygen peaks become increasingly important in Figures 9 and 10, implying higher ambient densities for these species than are predicted by the ambient density model of reference 16. High molecular oxygen values were also observed during preflight calibration of the mass spectrometer in the high velocity O-atom beam at Los Alamos National Laboratories and is attributed to O-atom recombination in the ion source. O/O_2 peak area ratios were very nearly the same on orbit and at Los Alamos.

Mass spectra corresponding to deep wake orientation at the same altitudes are shown in Figures 11 and 12. Water vapor is the only prominent peak in all spectra and the total pressure is obviously much lower (see scale on vertical axis). No significant amount of AO, molecular nitrogen or molecular oxygen is apparent.

Mass spectrometers measure the density of gas in the ion source, so we can calculate the density of various species in the ram and wake spectra (using the thermal gas calibrations of the mass spectrometer, not the high velocity neutral beam calibration) and compare with the values calculated by Runflux (ref. 16) (Table 3). As inspection of Table 3 shows the ram spectra contain higher N_2 and O_2 than is predicted by the MSIS-86 model. The high O_2 levels result from recombination of AO in the instrument, and the orbital data show the same O_2/O peak area ratios that were observed in the preflight calibration with the high velocity neutral O-atom beam at Los Alamos.

The most important discrepancy between the MSIS-86 model and the mass spectrometer measurements is found in the N_2/O partial pressure ratio which is too large to account for with either the well-known dependence of vacuum pumping speed on atomic or molecular mass (ref. 17). Replacing the partial pressure of O with $O+O_2$ still leaves a big discrepancy. Argon, however, shows a similar excess while nitrogen to argon ratios appear normal. Simultaneous and nearly equal enhancements of argon and nitrogen suggest the occurrence of magnetic storm conditions during EOIM-III (personal communication, Dr. Alan Hedin). Data from the National Oceanics and Atmospherics Administration Space Environment Services Center show that the daily A_p index changed from 5 to 43 during STS-46 while the daily F10.7 increased from 103 to 141. A modified version of the Runflux method (ref. 16) which employs 3-h average values of geomagnetic indices, should be able to calculate the observed nitrogen and argon levels. The results of calculations with the modified Runflux model will be reported in a subsequent publication.

Mass spectrometric measurements of the induced environments in the carousel sectors contain evidence of gas scattering off cargo bay and experiment surfaces, though the primary objectives of the carousel measurements could be achieved nonetheless. A comparison of the mass spectra taken with and without the carousel baffle over the ^{13}C Kapton coated sector shows the clear presence of $^{13}CO_2$ and ^{13}C ions in the carousel spectra as shown in Figures 13 and 14. ^{12}CO is probably also present but cannot be resolved the N_2 peak as both are at mass 28.

The effects of engine firings were often apparent in the ambient ram mass spectra. Especially interesting was the appearance of a mass peak corresponding to NO after Primary Reaction Control System (PRCS) engine firings which decayed in intensity with a characteristic time of about a minute. The NO appears to be desorbing from orbiter surfaces long after the 80-ms engine pulse has been terminated. A typical mass spectrum taken shortly after a pulsed PRCS firing in the -Z direction is shown in Figure 15.

It should be obvious from the preceding paragraphs that quantitative interpretation of the EOIM-III mass spectrometer data, including final high accuracy estimates of the oxygen atom

fluence, will require more detailed modeling of both the ambient and the induced environment in the space shuttle cargo bay. That modeling effort is in progress and results will be published at a later date.

Polymeric Materials Reactivity

The measured reaction efficiencies (cm^3 of material removed per O-atom) of the JSC polymeric materials samples from the EOIM-III passive trays are shown in Table 4 (hydrocarbons and inorganics) and Table 5 (halocarbons), along with reaction efficiencies produced by previous flight experiments if the data exist. The passive tray reaction efficiencies produced by EOIM-III are in reasonable agreement with the results of earlier in-space experiments. Reaction efficiencies were calculated using the Runflux (ref. 16) with monthly average values (July, 1992) of A_p and F10.7 to estimate O-atom fluence in all cases. We believe these values are about 10 to 20 percent too low as a result of the large change in solar activity parameters which occurred during the 42-h exposure period. More accurate atom fluences and reaction efficiencies will be reported as they become available. No previous in-space data were available for many of the polymers flown on EOIM-III.

Scanning electron photomicrographs of Kapton-HN™ samples from STS-41 (INTELSAT Solar Array Coupon, 1.1×10^{20} O-atoms/cm^2) (ref. 6) and STS-46 (EOIM-III, 2.07×10^{20} O-atoms/cm^2) are compared in Figures 16 and 17, respectively. The familiar carpet or grass morphology produced by high velocity O-atom attack is evident in both photomicrographs (Kapton-HN™ itself is relatively smooth and featureless at these magnifications). The measured reaction efficiencies were 3.3×10^{-24} cm^3/atom for STS-41 and 3.5×10^{-24} cm^3/atom for STS-46, demonstrating the near equivalence of the cargo bay exposure of EOIM-III and the remote manipulator system (RMS) exposure (samples were exposed to ram about 10 m away from the cargo bay) of STS-41.

The effects of the long solar inertial period prior to EURECA deployment (Table 1) is apparent in the reactivity of the FEP and TFE Teflon™ samples (Table 5). While considerably lower than the reaction efficiencies measured on Solar Max satellite repair samples or on the LDEF, the EOIM-III reaction efficiencies of FEP and TFE Teflon™ are significantly higher than those measured on STS-8 (EOIM-II) or on STS-41. It is likely that the differences in the reactivity of the Teflons™ in these missions is due to differences in the net solar UV/VUV dose as has been suggested by both ground based testing (ref. 18) and detailed analysis of LDEF materials (ref.19).

Tables 4 and 5 show some interesting general trends in the reactivity of polymers as a function of molecular structure. Eymyd-F™, a polyimide similar to Kapton-HN™ but with all hydrogen atoms replaced by fluorine atoms (during synthesis, not as a result of surface fluorination after synthesis), shows the same reaction efficiency as Kapton™, demonstrating that the same reactivity is obtained in these aromatic systems whether hydrogen or fluorine is bonded to the aromatic ring carbons. It is also the case that the saturated hydrocarbons, as a group, (polyethylene, polypropylene, polymethylpentene) show significantly higher reaction efficiencies than the aromatic polymers with the notable exception of polycarbonate. The unusually high reaction efficiency of polycarbonate may be related to the well-known radiation sensitivity of that material though the mechanistic details are unclear at this time. Radiation sensitivity and O-atom reactivity may be related mechanistically. We do not, however, mean to suggest that the high reaction efficiency was necessarily caused by the space radiation dose received during STS-8 or STS-46.

As shown in Table 4, passive tray reaction efficiencies of a wide variety of polymer types fall within a factor of 1.5 of the average value for the group. Changes in polymer molecular structure which produce enormous changes in general physical and chemical properties produce only small changes in O-atom reactivity in LEO for this set of polymers. It should be noted that polystyrene, polybenzimidazole, and polysulfone showed reaction efficiencies somewhat lower than this group during STS-8, but still within a factor of 2 of the mean value of the EOIM-III group reported above.

In contrast, comparison of the simple saturated hydrocarbons, i.e. polyethylene, polypropylene, and polymethylpentene, with FEP Teflon™, TFE Teflon™, Tefzel™, and Kynar™ show that the presence of C-H bonds determines the reactivity of these saturated systems in which hydrogen atom abstraction is an important step in the overall mass loss reaction. Tefzel™ and Kynar™, which contain equal numbers of C-H and C-F bonds in the polymer repeat unit, show reactivity intermediate between polyethylene and the Teflons™. It should be noted that the C-H bond is much stronger in Tefzel™ and Kynar™ than it is in polyethylene suggesting that H-atom abstraction will be correspondingly more difficult. In addition, Tefzel™ and Kynar™ have only half as many C-H bonds available for direct O-atom attack.

The saturated chain hydrocarbon polymers, polyethylene, polypropylene, and polymethylpentene have the highest observed reaction efficiencies (except for polycarbonate). An important feature of the O-atom chemistry of these polymers is the production of highly reactive gas phase reaction products such as O-H radical which have been observed to produce much higher rates for the saturated hydrocarbon polymers than for aromatic polymers such as Kapton™ and Mylar™ in thermal atom systems (ref. 20). The carpet morphology produced by high velocity O-atom attack on polymers results in a higher probability that any reactive gas phase product can recontact the polymer surface and react. This may be the best explanation for the relatively high O-atom reaction rates observed for the saturated hydrocarbon polymers both on-orbit and in the laboratory.

There is no definitive kinetic isotope shift between the fully deuterated polyethylene and the other polyethylenes as predicted for high by Koontz et al. (ref. 20) for the case of orbital velocity oxygen atoms. A deuterium kinetic isotope shift has been observed for thermal energy oxygen atoms(0.04 eV) reacting with polyethylene (ref. 20). The presence of a kinetic isotope shift at thermal energies combined with the disappearance of that shift at orbital energies (5 eV) suggests that much of the atom kinetic energy is directly available to overcome the activation barriers to O-atom reactions with polyethylene and suggests that H atom abstraction is the rate limiting step of the reaction at thermal atom energies.

It is interesting to note that one previously untested (in-space) polymer, the poly(bistrifluoropropylphosphazene), shows little or no mass loss or other signs of degradation either in the passive trays or in the heated trays (see below), verifying the predictions of ground based testing (ref. 21). This polymer may have value as an elastic protective coating or as a durable elastomer for use in O-atom environments.

Temperature dependence of the O-atom reactivity of polymeric materials was an important secondary objective of EOIM-III. The results of the heated tray subexperiment are summarized in Table 6, where the data are expressed as parameters of the Arrhenius equation,

$$R = A \times e^{-(E_a/kT)}$$

where R is the rate of reaction expressed as reaction efficiency at constant atom flux, A, the pre-exponential factor, is equal to the absolute rate at high temperatures ($kT > E_a$), E_a is the activation

energy or activation barrier size, k is the Boltzman constant, and T is the temperature, the heated tray temperature in this case. The kinetic energy of the high velocity ram oxygen atoms (5 eV) does not appear in this expression and, significantly, the activation energies measured in a number of thermal atom (0.04 eV) systems are on the order of 10 times larger (ref. 20) implying that some portion of the atom kinetic energy is available for overcoming activation barriers in the rate limiting step of the process, as was suggested in the discussion of kinetic isotope shifts in polyethylene discussed above.

SUMMARY AND CONCLUSIONS

The primary and secondary data objectives of the EOIM-III flight experiment were achieved during STS-46. The preliminary data analysis and interpretation presented in this paper demonstrate that the overall objectives of EOIM-III can be achieved with more detailed analysis of the flight data and flight samples. In a qualitative sense, those overall objectives have already been achieved and demonstrated. More accurate Runflux calculations combined with a complete postflight calibration check of the mass spectrometer will be completed in the near future, permitting quantitative completion of the EOIM-III objectives.

The EOIM-III materials reactivity measurements have, in combination with the mass spectrometer data, increased our confidence in the existing materials reactivity data base as well as expanding that data base significantly by producing: (1) reaction efficiency data on previously untested polymers showing remarkable durability, (2) activation energy (temperature dependence) data on a range of polymers, and (3) new reaction mechanism data which confirms the fundamental importance of chemistry in understanding the reactivity of materials in the LEO environment. These results suggest that thermal energy O-atom Arrhenias parameters can be used to estimate orbital energy O-atom reactivities in some cases, thereby improving our confidence in low cost thermal atom screening tests. In addition, the EOIM-III data provide a foundation for validating high quality laboratory simulations of the LEO environment as well as supporting materials test method development.

In addition, the mass spectrometer data provide a unique resource for improving our understanding of vehicle-environment interactions in the LEO environment. Direct measurements of ambient neutral and ionic species sampled with various vehicle attitudes and mass spectrometer orientations permit direct verification of induced environment models. More complete results of EOIM-III will be published as data reduction and analysis is completed.

REFERENCES

1. Jursa, A.S., editor: "Handbook of Geophysics and the Space Environment." Air Force Geophysics Laboratory, United States Air Force, 1985 (National Technical Information Service).

2. Griffin, M.D., and French, J.R.: "Space Vehicle Design." Chapter 3, Environment; AIAA, Washington, DC, 1991.

3. Hedin, A.E.: "A Revised Thermospheric Model Based on Mass Spectrometer and Incoherent Scatter Data: MSIS-83." J. Geophys. Res., vol. 88, No. 10, 1983, pp. 170–188.

4. Visentine, J.T., Leger, L.J., Kuminecz, J.F., and Spiker, I.K.: "STS-8 Atomic Oxygen Effects Experiment." AIAA paper AIAA-85-0415, 23rd Aerospace Sciences Meeting, January 14–17, 1985, Reno, NV.

5. Zimcik, D.G., and Magg, C.R.: "Results of Apparent Oxygen Reactions with Spacecraft Materials During STS-41G." J. Spacecraft, vol. 25, No. 2, March–April 1988.

6. Koontz, S., King, G., Dunnet, A., Kirkendahl, T., Linton, R., and Vaughn, J.: "The International Telecommunications Satellite (INTELSAT) Solar Array Coupon (ISAC) Atomic Oxygen Flight Experiment: Techniques, Results and Summary." Materials in a Space Environment, September 1991, Tolouse, France, Publisher, Centre National D'Etudes Spatiales, Tolouse, 1992.

7. Visentine, J.T., comp.: "Atomic Oxygen Effects Measurements for Shuttle Missions STS-8 and STS-41G, Volumes I to III." NASA Technical Memorandum 100459.

8. Leger, L.J., Visentine, J.T., and Santos-Mason, B.: "Selected Materials Issues Associated With Space Station *Freedom*." SAMPE Quarterly, vol. 18, No. 2, January 1987, pp. 48–54.

9. Mende, S.B., Swenson, G.R., Clifton, K.S., Gause, R., Leger, L. J., and Garriot, O. K.: "Space Vehicle Glow Measurements on STS-41D." J. Spacecraft, vol. 23, No. 2, March–April, 1986, pp. 189–193.

10. Banks, P.M., and Williamson, P.R.: "Space Shuttle Glow Observations." Geophys. Res. Lett., vol. 10, 118, 1983.

11. Swenson, G.R., and Meyerott, R.E.: "Spacecraft Ramcloud Atom Exchange and N_2 LBH Glow," Geophys. Res. Lett., vol. 15, No. 3, pp. 245–248.

12. Hedin, A.E.: "MSIS-86 Thermospheric Model." J. Geophys. Res., vol. 92, No. A5, May 1987, pp. 4649–4662.

13. Visentine, J.T., and Leger, L.J.: "Materials Interactions With the Low-Earth Orbit Environment: Accurate Reaction Rate Measurements." AIAA paper AIAA 85-7019, AIAA Shuttle Environments and Operations II Conference, November 1985, p. 168.

14. Hunton, D.E., Trzcinski, E., Wlodyka, L., Federico, G., and Dorian, J. 1Lt, USAF: "Quadrupole Ion-Neutral Mass Spectrometer for Space Shuttle Applications." AFGL-TR-86-0084, Environmental Engineering Paper No. 953.

15. Koontz, S.L., Cross, J.B., and Lan, E.: "Characterization and Calibration of the EOIM-III Flight Mass Spectrometer in a High Velocity Atom Beam." Materials Degradation in Low-Earth Orbit (LEO), Srinivasan, V., and Banks, B. A., eds., The Materials, Metals and Minerals Society, 1990.

16. Leger, L.J., Visentine, J.T., and Schleising, J.A.: "A Consideration of Atomic Oxygen Interactions with Space Station." AIAA-85-0476, AIAA 23rd Aerospace Sciences Meeting, January 14–17, 1985, Reno, NV.

17. Santeler, D., and Warren, D.: "Computer Solution to Chamber-Gas Fractionation During Pumpdown." J. Vac. Sci. Technol. A11(1), January–February 1993, pp. 231–239.

18. Koontz, S.L., Leger, L.J., Albyn, K.A., and Cross, J.: "Ultraviolet Radiation/Atomic Oxygen Synergism in Materials Reactivity." J. Spacecraft, vol. 27, No. 5, May–June 1990, pp. 346–348.

19. Steigman, A.E., Brinza, D.E., Anderson, M.S., Minton, T.K., Laue, E.G., and Liang, R.H.: "An Investigation of the Degradation of Fluorinated Ethylene Propylene (FEP) Copolymer Thermal Blanketing Materials Aboard LDEF and in the Laboratory." JPL publication 91-10, May 15, 1991, Jet Propulsion Laboratory, Pasadena, CA.

20. Koontz, S.L., Albyn, K., and Leger, L.J.: "Atomic Oxygen Testing with Thermal Atom Systems: A Critical Evaluation." J. Spacecraft, vol. 28, No. 3, May–June 1991, pp. 315–323.

21. Fewell, L., and Fenney, L.: Polymer Comm., vol. 32, No. 13, 1991, pp. 393–396.

Table 1. STS-46 AO fluence summary.

	Orbiter Altitude, Nmi	Exposure Attitude	Exposure Duration, (H)	AO Fluence, Atoms/cm^2
• EURECA Deployment & Checkout	231	-ZSI	11.27	3.29×10^{17}
• EURECA Release & Station Keep	231	-ZVV	5.28	6.45×10^{17}
• EOIM-3 Flight Operations	124	-ZVV	42.25	2.06×10^{20}
AO Total Fluence:			58.80	2.07×10^{20}

Table 2. EOIM-III XPS survey results.

- X-ray photoelectron spectroscopy: Pre- and postflight surface contamination measurements
  - Payload hardware and some sample materials were analyzed by XPS (KSC/Dr. Orlando Melendez)
  - No evidence of fluorocarbon contamination (<0.5 atom percent fluorine) on nonfluorocarbon samples tested
  - Surface silicon was detected as silicate
  - Polymer samples: O atom percent on covered portions; 0.8 to 2.39 atom percent on AO exposed surfaces
  - For exposed hardware, average is 5.95 (±3.8) atom percent SI, pure SiO_2 is 30 atom percent Si. Exposed hardware samples not corrected for natural Si content.
- Conclusion: Surface contamination nominal.

Table 3. RUNFLUX ambient versus mass spec. ram/wake densities.

Gas	alt. (nmi.)	Mass spec. ram (atoms or molecules per cc)	Mass spec. wake (atoms or molecules per cc)	Ave. MSIS-86 (atoms or molecules per cc)
O	231	3.2×10E9	———	5.0×10E7
H_2O		2.8×10E9	———	0.0
N_2		3.0×10E9	———	2.3×10E6
O_2		9.3×10E8	———	5.5×10E4
CO_2		8.7×10E8	———	0.0
O	160	6.3×10E10	5.0×10E8	3.6×10E8
H_2O		5.4×10E9	3.9×10E8	0.0
N_2		5.7×10E10	6.4×10E8	1.6×10E7
O_2		3.9×10E10	1.8×10E8	3.9×10E5
CO_2		7.8×10E9	2.1×10E8	0.0
O	124	1.7×10E11	4.5×10E8	2.2×10E9
H_2O		2.2×10E9	3.6×10E8	0.0
N_2		3.6×10E11	0.0	4.9×10E8
O_2		2.5×10E11	0.0	6.3×10E7
CO_2		3.3×10E9	0.0	0.0

Table 4. Reaction efficiencies* (RE) ($\times 10^{24} cm^3$ /atom)
1-inch samples: passive trays.

POLYMER	RE (EOIM-III)	RE (STS-8)
Eymyd-F Polyimide (Ethyl Corp.)	3.0	
CR-39 Polycarbonate	7.0	6.0
LCP 4100 (liquid crystal, DuPont)	3.7	
XYDAR (liquid crystal, Amoco Chemical)	3.3	
VICTRIX PEEK (ICI)	3.9	
POLYMETHYLPENTENE	6.1	
HDPE EMH6606 (Phillips)	4.3	3.7
"ROUND ROBIN" POLYETHYLENE	5.1	
DEUTERATED (D4) POLYETHYLENE	4.3	
MYLAR A (DuPont)	4.4	3.9
"ROUND ROBIN" KAPTON (DuPont)	3.5	3.0
POLYPHOSPHAZENE; X-221 (Ethyl Corp.)	$<5\times10^{-2}$	
EYPEL (R) – F GUM; X-222 (Ethyl Corp.)	$<5\times10^{-2}$	

* Reaction efficiencies calculated from sample weight loss and preliminary MSIS-86 AO fluence. Samples were vacuum-baked for 48 h prior to weighing both before and after flight.

Table 5. Reaction efficiencies* (RE) ($\times 10^{24} cm^3$ /atom)
1-inch samples: passive trays.

HALOCARBON POLYMER	RE (EOIM-III)	RE (STS-8)
TEFZEL BLUE (SSF WP-4, Raychem))	1.3	
TEFZEL WHITE (SSF WP-4, Raychem)	1.0	
POLYCHLOROTRIFLUOROETHYLENE	1.0	
"ROUND ROBIN" FEP TEFLON	5.6×10^{-2}	$<3\times10^{-2}$
PTFE	6.5×10^{-2}	
KYNAR (Penwalt)	1.4	
TEFZEL (DuPont)	1.0	
TEDLAR (DuPont)	4.3	3.2
ACLAR 33C (Allied)	1.1	
HALAR (Allied)	2.2	

* Reaction efficiencies calculated from sample weight loss and preliminary MSIS-86 AO fluence. Samples were vacuum-baked for 48 h prior to weighing both before and after flight.

Table 6. Polymer arrhenius activation parameters.

POLYMER	A (cm^3/atom$\times 10^{24}$)	E_a (eV)
Kapton (polyimide)	7	0.02
XYDAR (liq. crystal)	22	0.05
CR-39 polycarbonate	30	0.04
LCP 4100 (liq. crystal)	20	0.04
EYMIDE-F (fluroine substituted polyimide)	9	0.03
Mylar	7	0.05
Tefzel	2	0.04
HDPE (polyethylene)	13	0.06

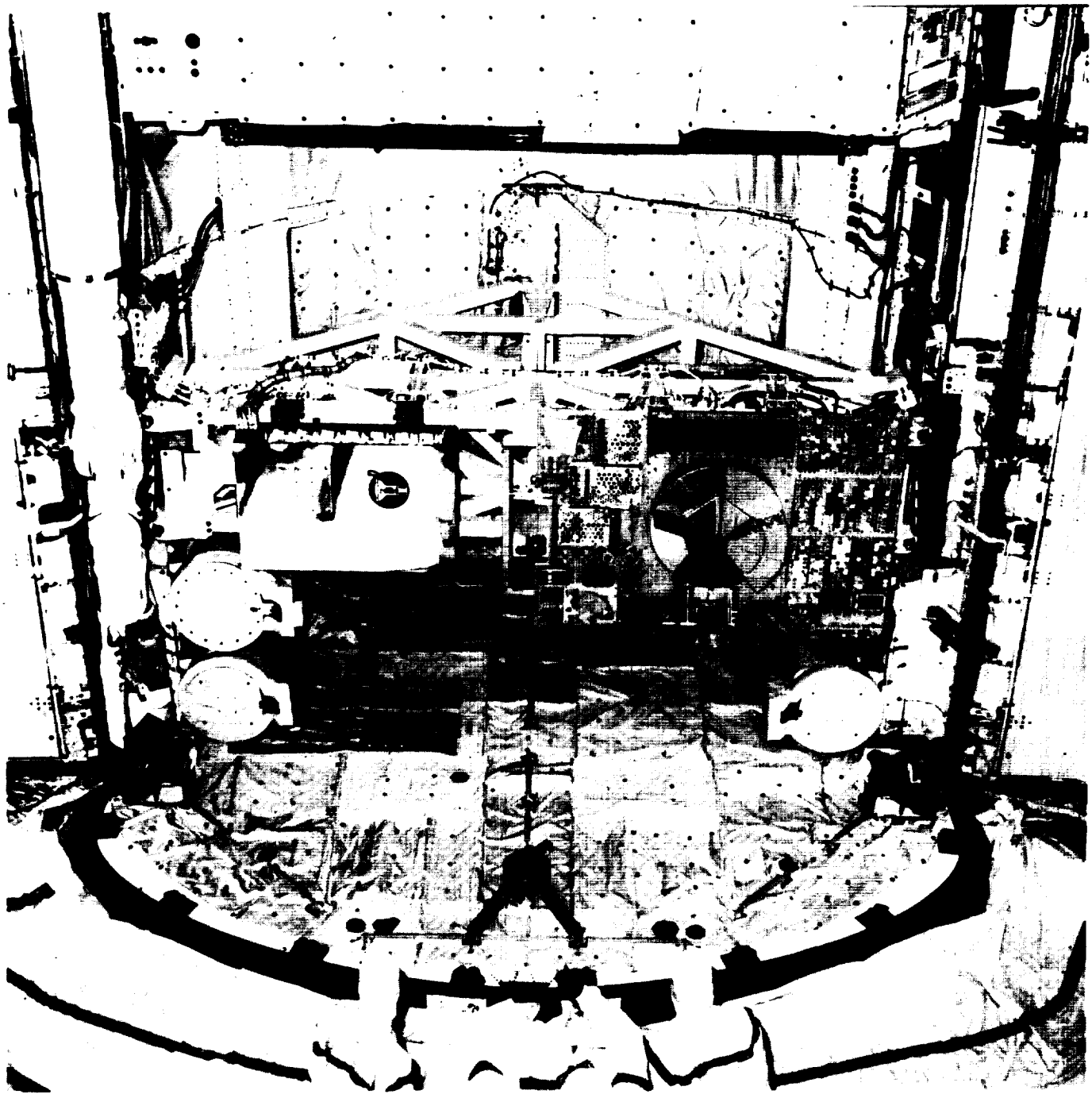

Figure 1. Launch pad close-out photo of EOIM-III (left) and TEMP-2A (right). The aft cargo bay bulkhead is visible at the top of the photo.

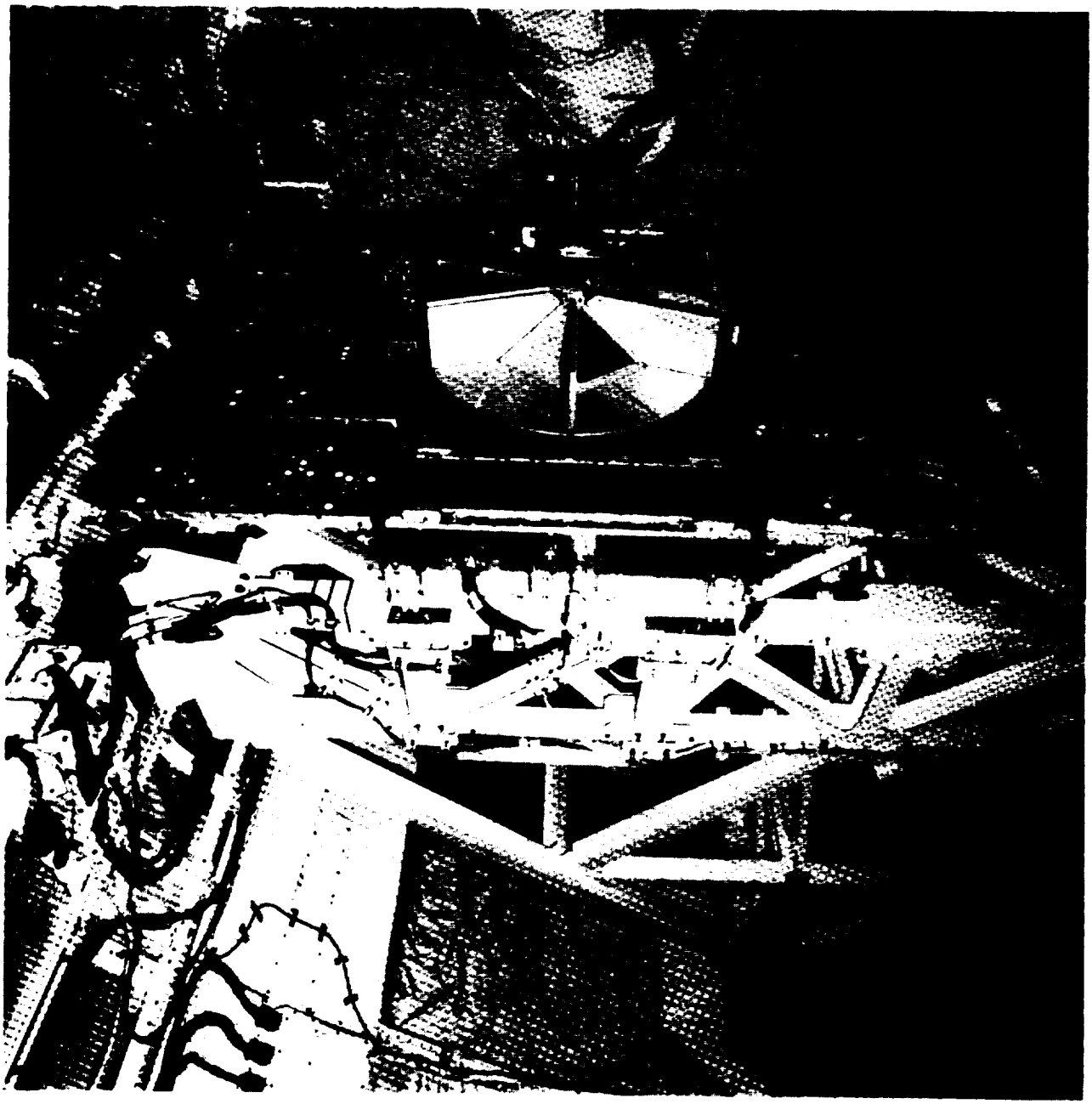

Figure 2. Launch pad close-out photo of EOIM-III payload looking toward the aft cargo bay bulkhead, i.e. the forward edge of the payload nearest the viewer in this photo.

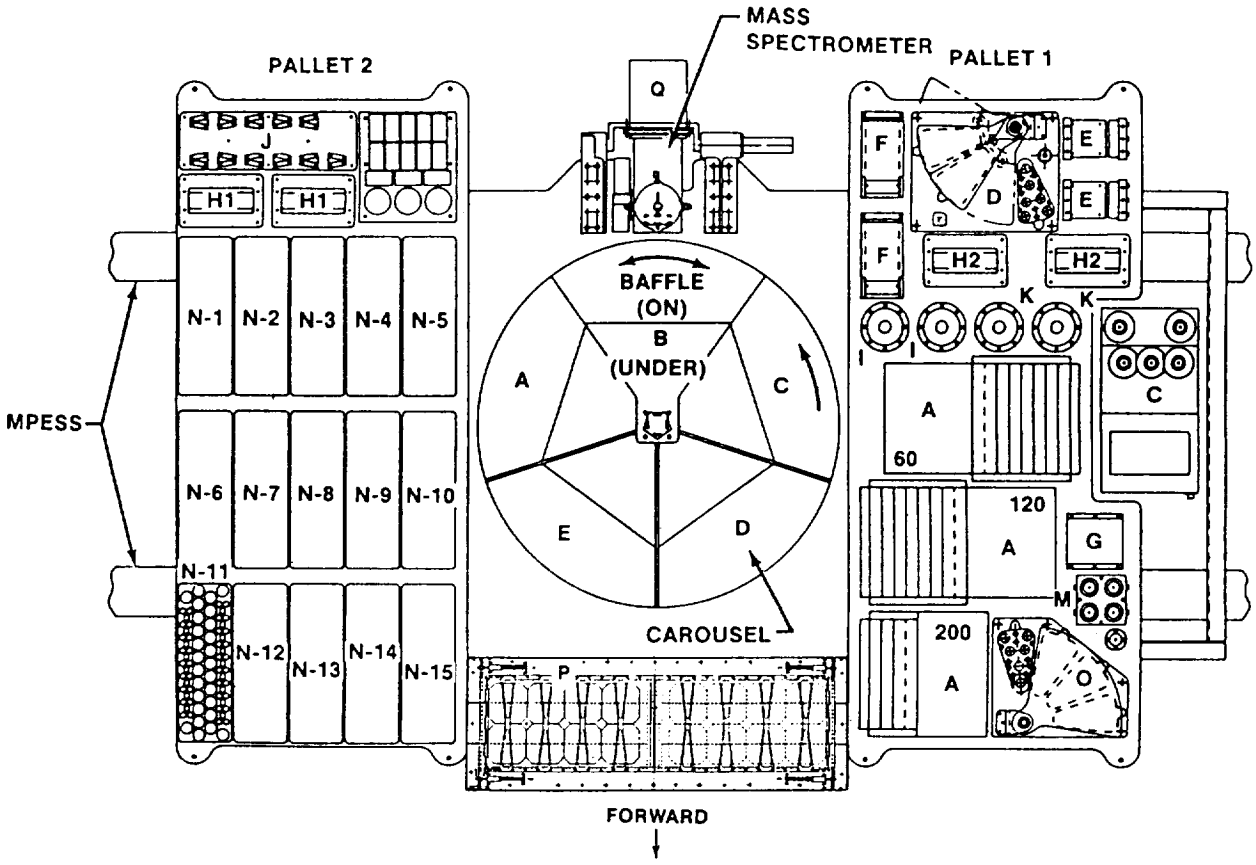

ATOMIC INTERACTION EXPERIMENTS:

A - HEATED PLATE (JSC), 3EA
B - ATOM SCATTERING EXPERIMENT (UAH), 1EA
C - ENVIRONMENT MONITOR PACKAGE (GSFC), 1EA
D - SOLAR UV EXPERIMENT (JSC), 1EA
E - STATIC STRESS FIXTURE (MSFC), 2 EA
F - UNIFORM STRESS FIXTURE (MSFC), 2 EA
G - ATOMIC OXYGEN MONITOR (MSFC), 1 EA
H1 - COMPOSITE STRESS FIXTURE(LaRC), 2EA
H2 - COMPOSITE STRESS FIXTURE (JSC), 2 EA
I - SCATTEROMETER (JPL), 2 EA
J - MECHANICAL STRESS FIXTURE (LeRC), 11 EA
K - REFLECTOMETER (LeRC), 2 EA
L - PINHOLE CAMERA (LeRC), 1 EA
M - SCATEROMETER(AEROSPACE CORP.), 1EA
N - PASSIVE SAMPLE CARRIERS, 15 EA
O - VARIABLE EXPOSURE TRAY, 1EA
P - FREEDOM ARRAY MATERIALS EXPOSURE EXPERIMENT(LeRC), 1 EA
Q - QUADRUPLE MASS SPECTROMETER, 1 EA

Figure 3. A line drawing of the EIOM-III payload identifying the various features in Figures 1 and 2. The forward edge of the payload is at the bottom of the line drawing.

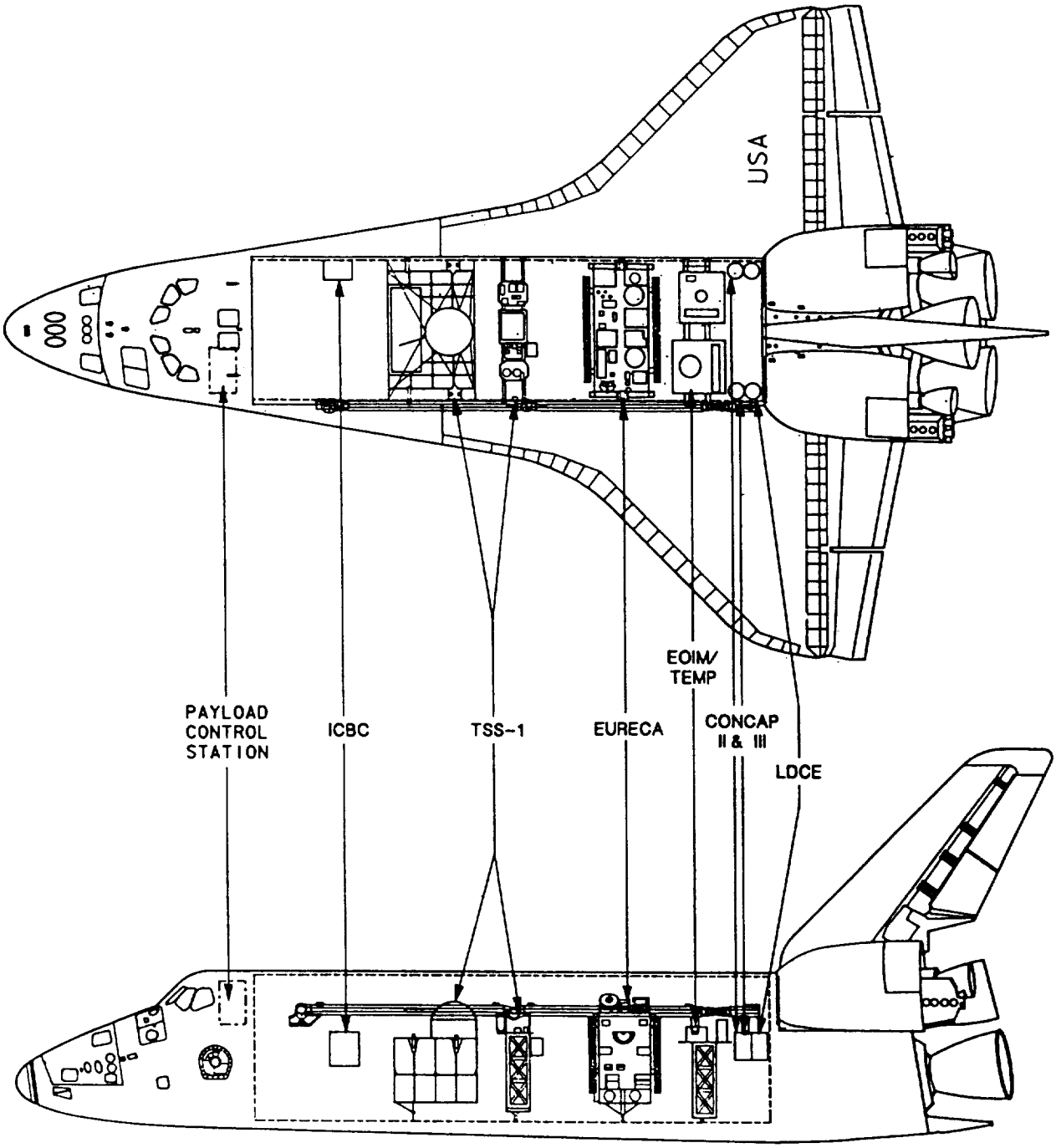

Figure 4. Cargo bay configuration of *Atlantis* for STS-46.

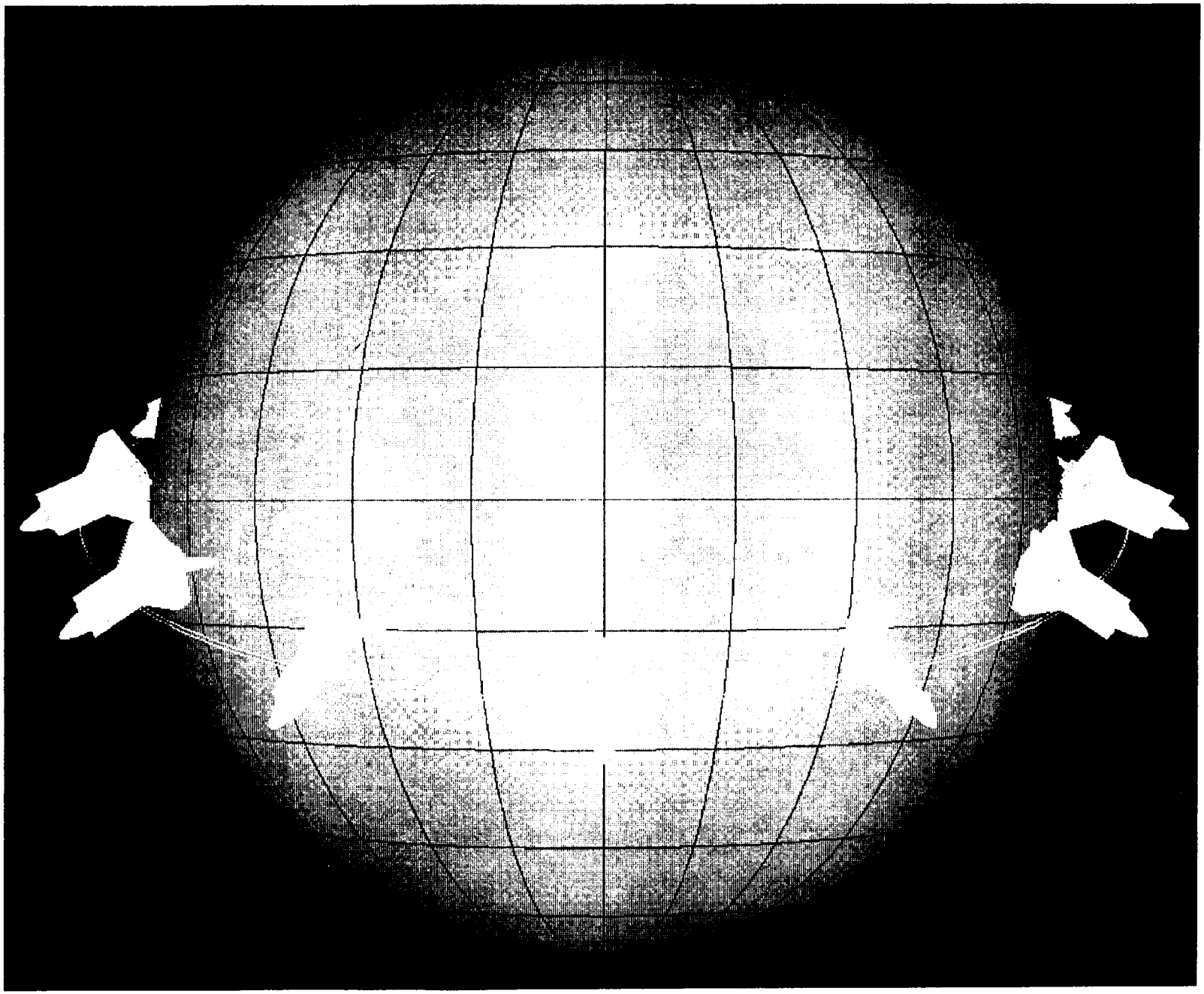

Figure 5. Orbital path and attitude of *Atlantis* during the 42-h EOIM-III period. The Sun-Earth vector is perpendicular to the center of the figure.

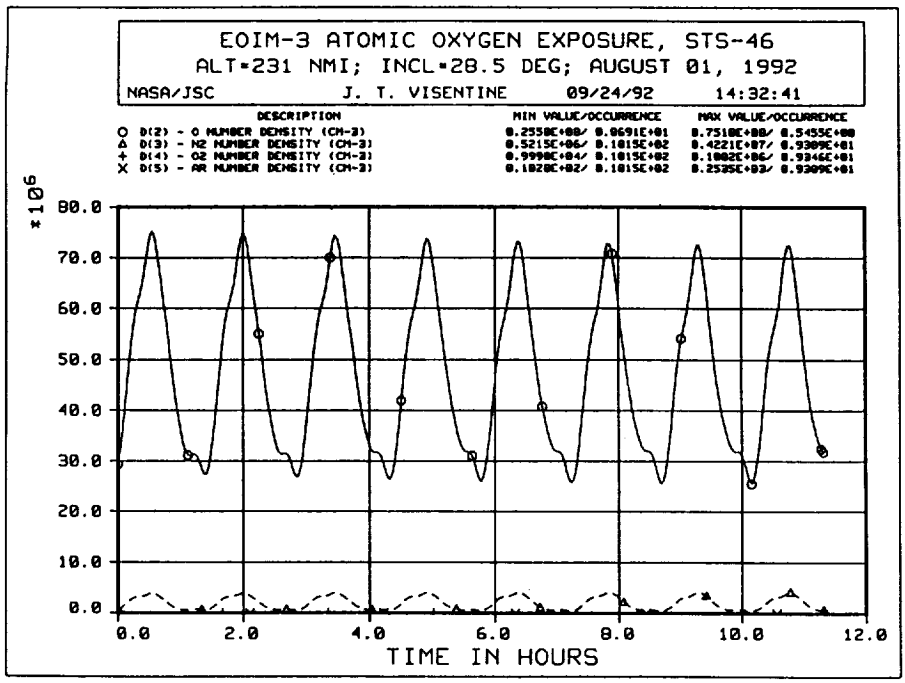

Figure 6. MSIS-86 predictions of O-atom density at 221 nmi.

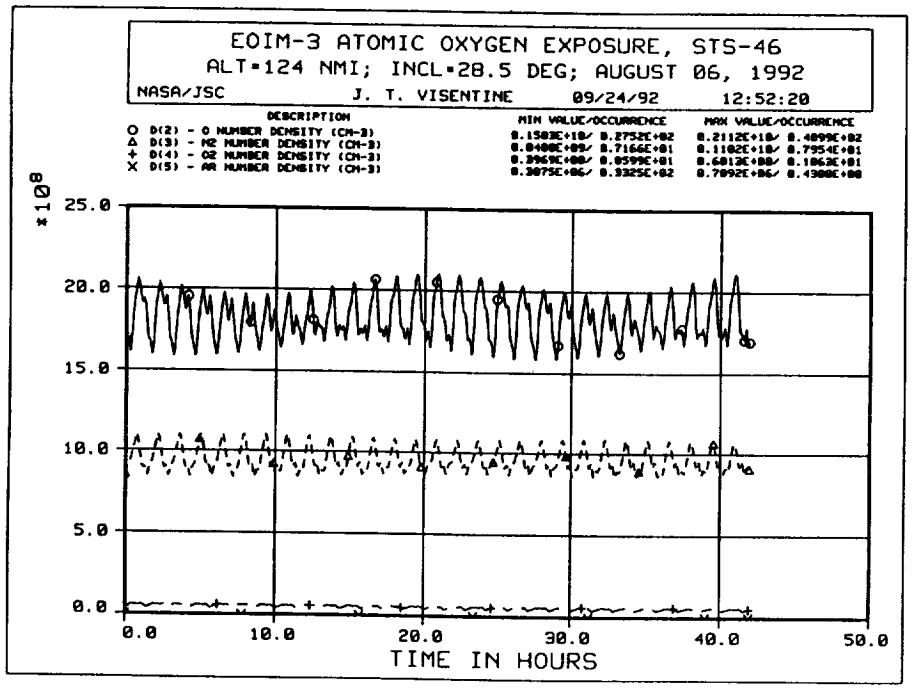

Figure 7. MSIS-86 predictions of O-atom density at 123 nmi.

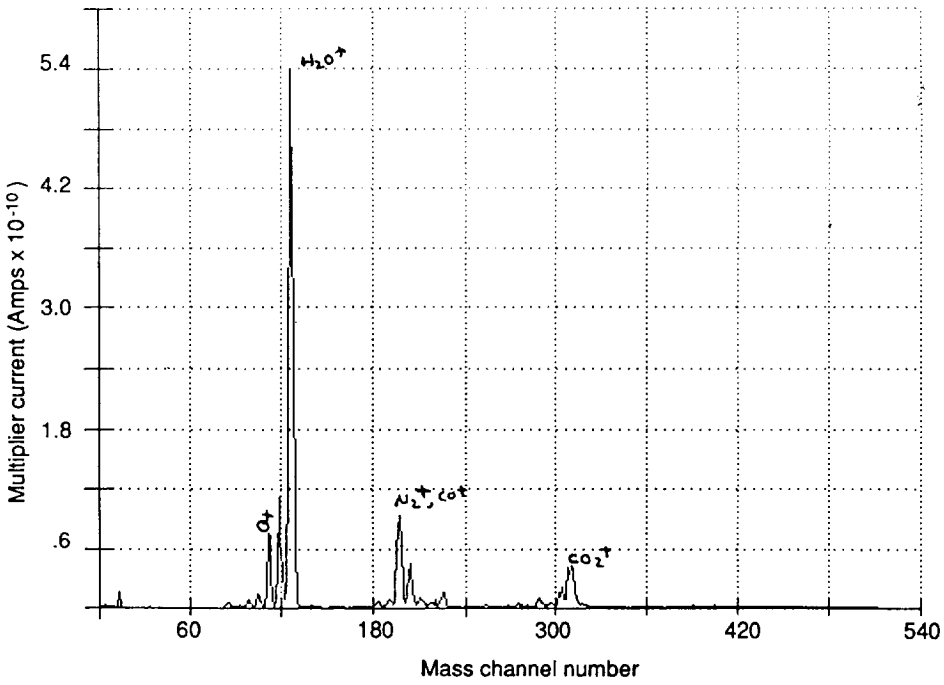

Figure 8. A typical neutral (mode 2) ram-flux mass spectrum taken at 231 nmi as part of the ambient density data set shown in Figure 6. *Atlantis* is in the -ZVV attitude; the mass spectrometer orientation is -Z, as in Figure 2.

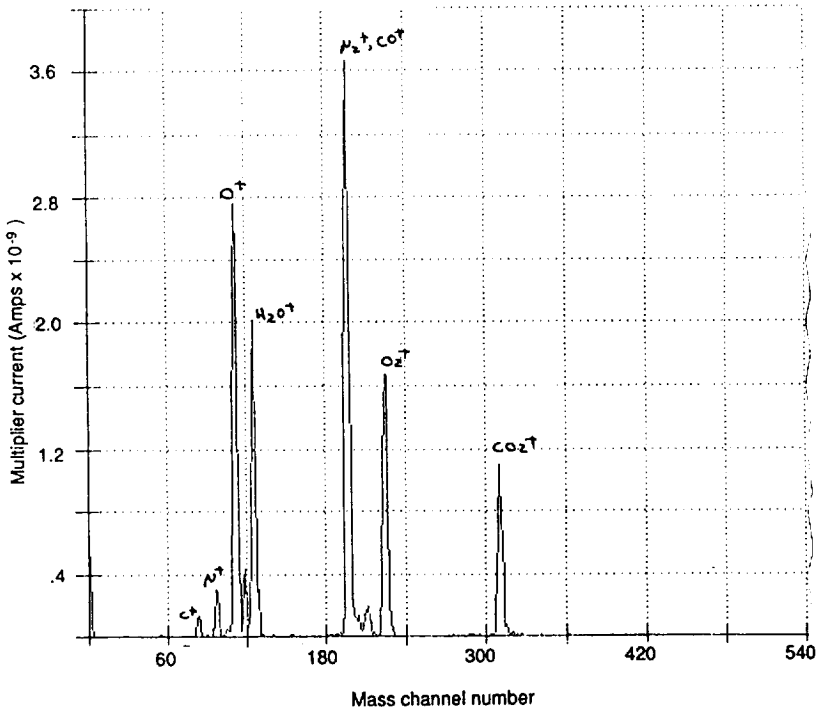

Figure 9. A typical neutral (mode 2) ram-flux mass spectrum taken at 160 nmi. *Atlantis* is in the -ZVV attitude; the mass spectrometer orientation is -Z, as in Figure 2.

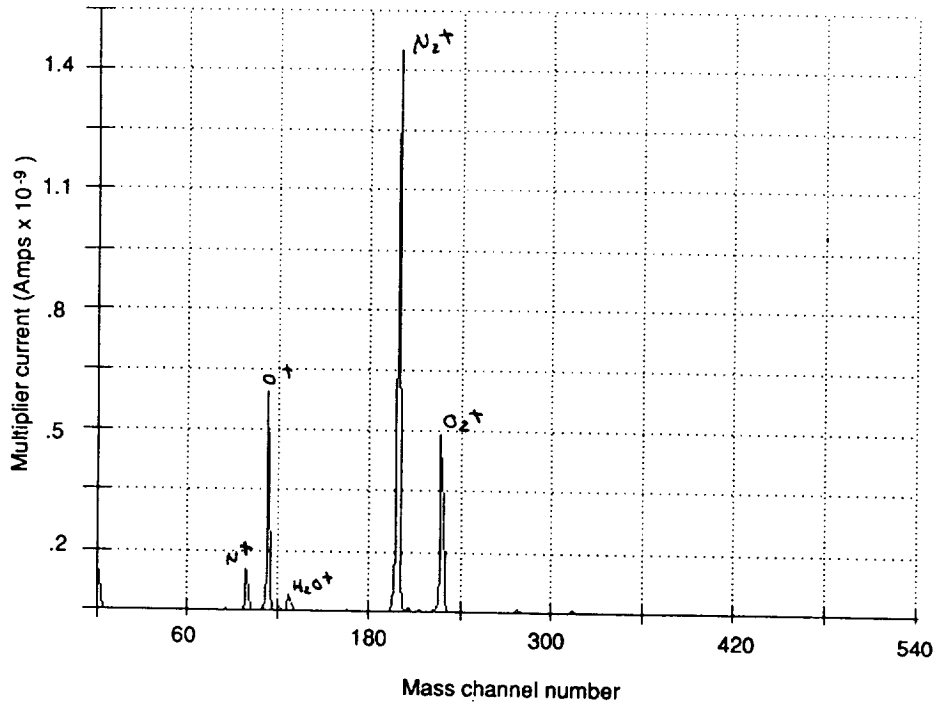

Figure 10. A typical neutral (mode 2) ram-flux mass spectrum taken at 123 nmi as part of the AO measurement sequence of the second preprogramming EOIM cycle. *Atlantis* is in the -ZVV attitude and the mass spectrometer is -Z oriented, as in Figure 2.

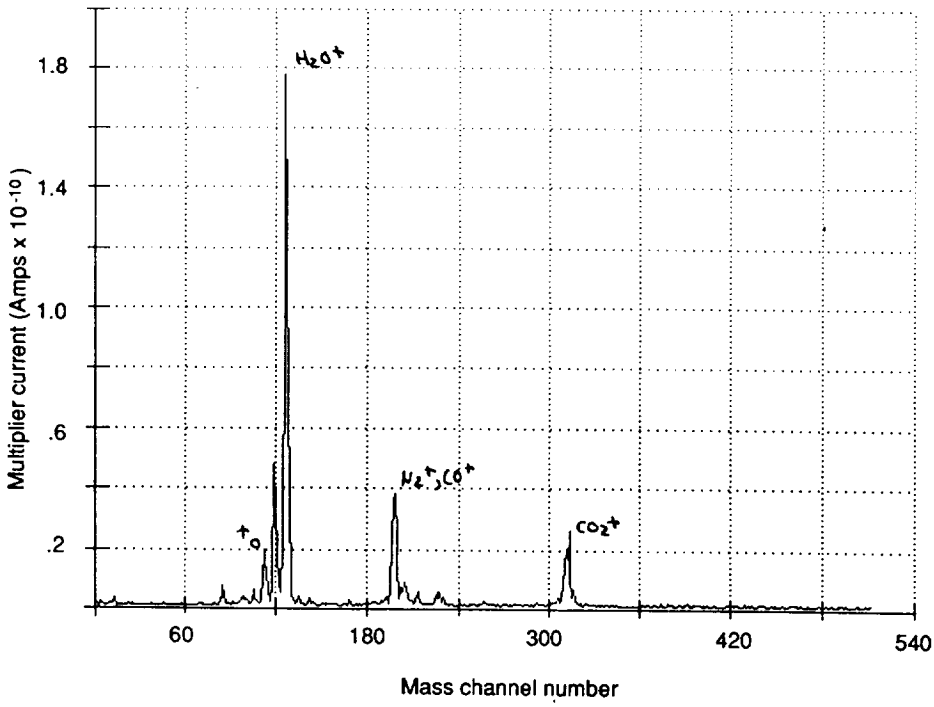

Figure 11. Deep wake mass spectrum taken with the same conditions as in Figure 9 except *Atlantis* is now +ZVV attitude (cargo bay in wake). The total pressure indicated is much lower than in the ram attitude, and the dominant mass peaks have changed.

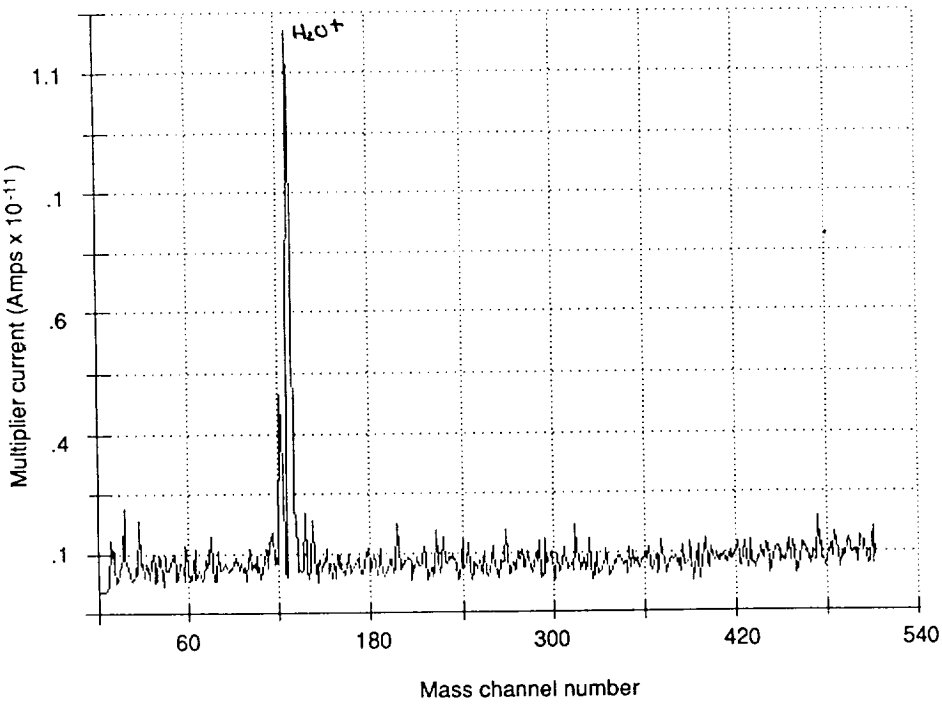

Figure 12. Deep wake mass spectrum taken with the same conditions as in Figure 10 except *Atlantis* is now +ZVV attitude (cargo bay in wake). The total pressure indicated is much lower than in the ram attitude, and the dominant mass peaks have changed.

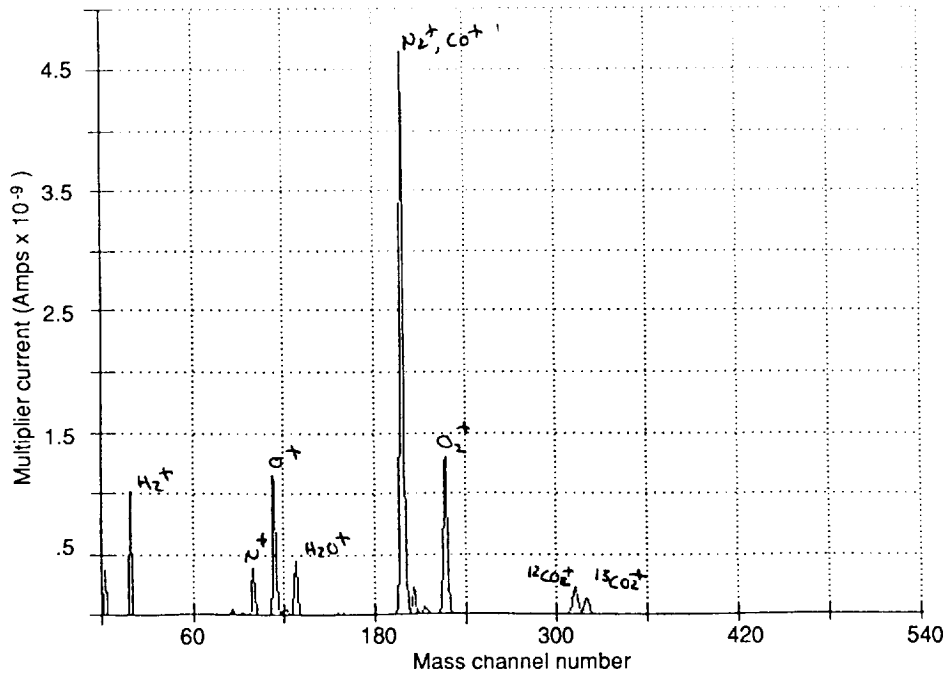

Figure 13. Mass spectrum of the gaseous induced environment above the carousel sector lined with ^{13}C Kapton. *Atlantis* is in the -ZVV attitude and the mass spectrometer is +X oriented. Direct ram ambient is incident on the carousel sector (baffle off). Isotopes labeled CO_2 and CO are both visible.

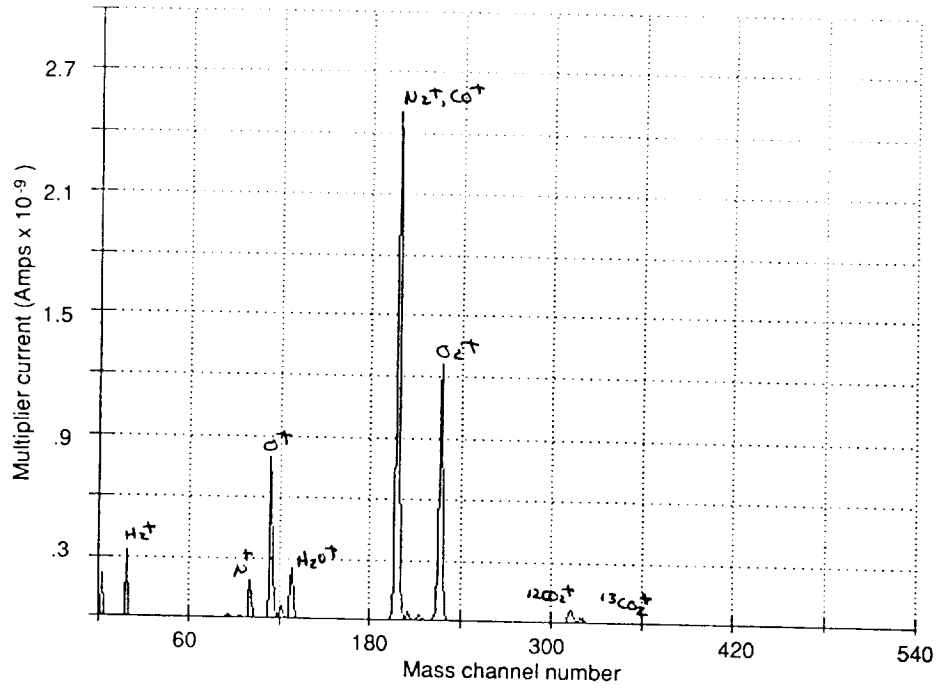

Figure 14. Mass spectrum of the induced environment in the carousel sector lined with ^{13}C Kapton™. Same conditions as Figure 13, except the baffle now covers the carousel sector under observation (baffle on). Some isotopes labeled CO and CO_2 are still visible, though the intensity is reduced.

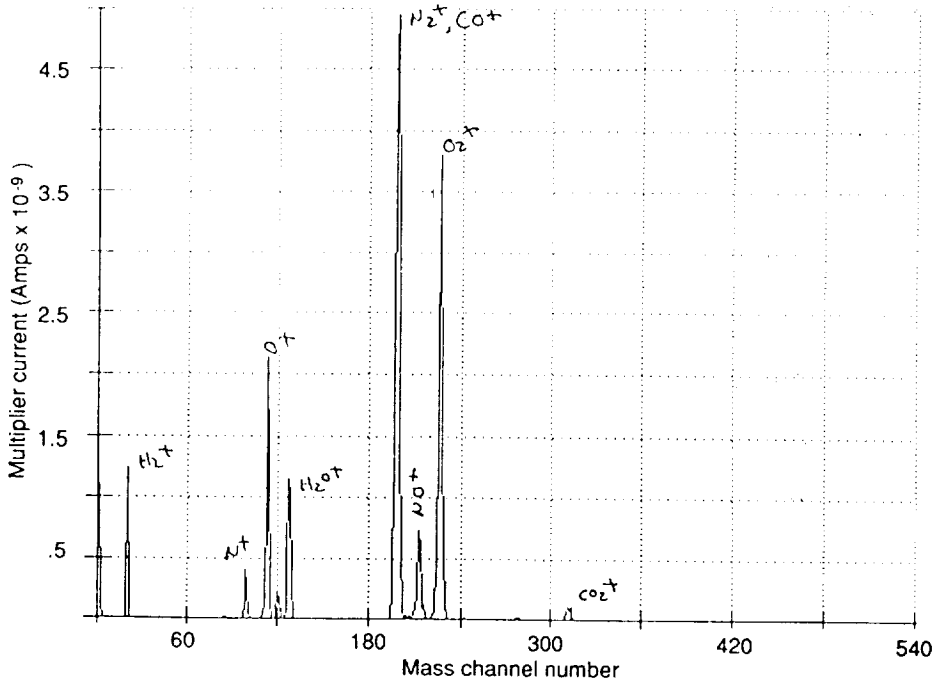

Figure 15. A typical mass spectrum taken shortly after an 80-ms pulsed firing of a -Z directed Primary Reaction Control System engine. The mass peak at 30 is believed to be NO and decays steadily after the engine pulse. This is an ambient ram mass flux spectrum, as in Figures 8 to 10.

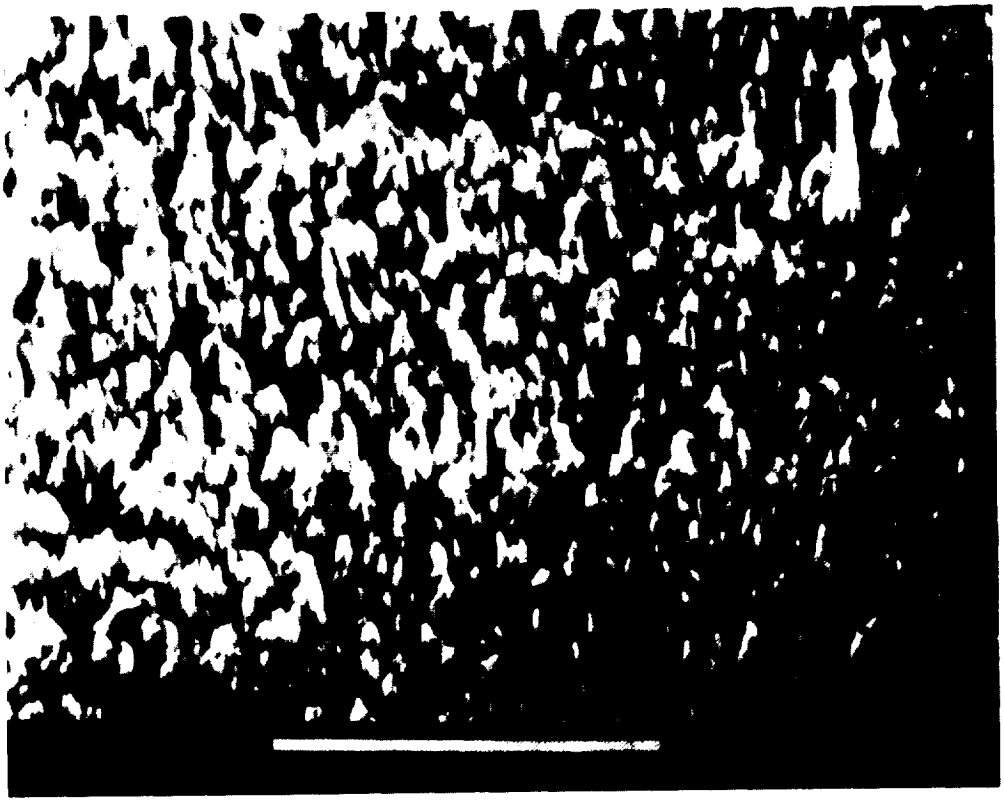

Figure 16. SEM photomicrograph of Kapton™ HN from EOIM-III passive sample tray.

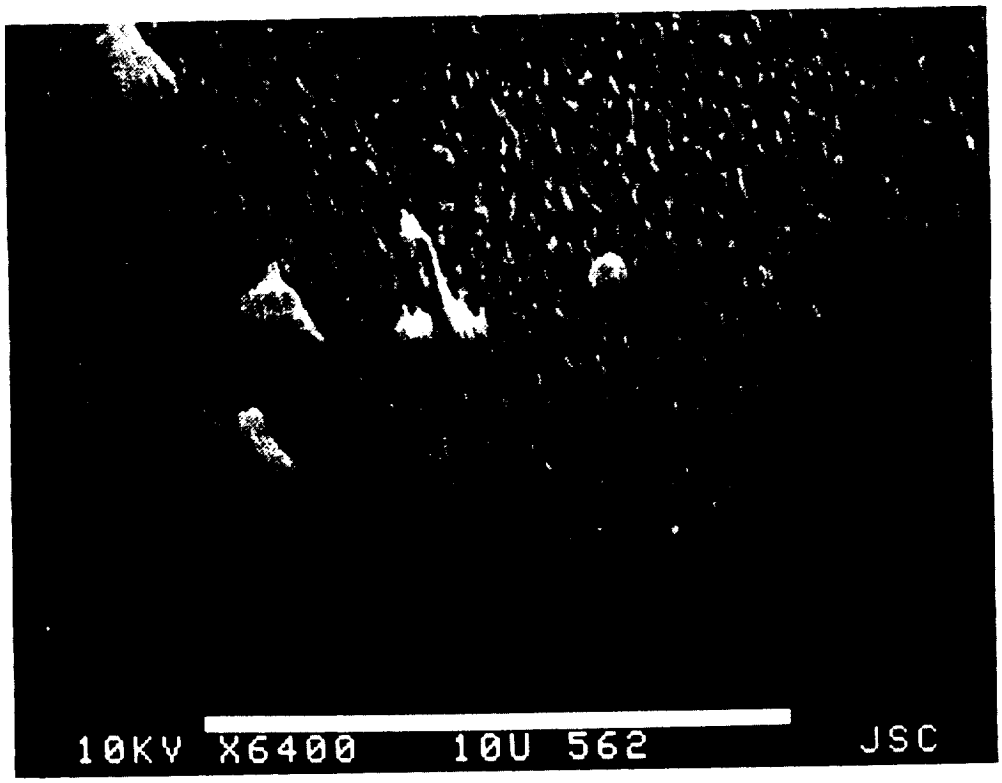

Figure 17. SEM photomicrograph of Kapton™ HN from ISAC sample tray (STS-41).